doi:10.1006/jmbi.2001.4852 available online at http://www.idealibrary.com on IDEAL J. Mol. Biol. (2001) 311, 297–310

JMB

Structure and Mechanism of the RuvB Holliday Junction Branch Migration Motor

Christopher D. Putnam[1], Sheila B. Clancy[1], Hiro Tsuruta[2] Susana Gonzalez[3], James G. Wetmur[3] and John A. Tainer[1]*

[1]*Department of Molecular Biology, Skaggs Institute for Chemical Biology, The Scripps Research Institute, MB 4 10550 North Torrey Pines Rd La Jolla, CA 92037, USA*

[2]*Stanford Synchrotron Radiation Laboratory/Stanford Linear Accelerator Center Stanford University, P.O. Box 4349, MS 69, Stanford CA 94309-0210, USA*

[3]*Department of Microbiology Box 1124, Mount Sinai School of Medicine, New York NY 10029-6574, USA*

*Corresponding author

The RuvB hexamer is the chemomechanical motor of the RuvAB complex that migrates Holliday junction branch-points in DNA recombination and the rescue of stalled DNA replication forks. The 1.6 Å crystal structure of *Thermotoga maritima* RuvB together with five mutant structures reveal that RuvB is an ATPase-associated with diverse cellular activities (AAA + -class ATPase) with a winged-helix DNA-binding domain. The RuvB-ADP complex structure and mutagenesis suggest how AAA + -class ATPases couple nucleotide binding and hydrolysis to interdomain conformational changes and asymmetry within the RuvB hexamer implied by the crystallographic packing and small-angle X-ray scattering in solution. ATP-driven domain motion is positioned to move double-stranded DNA through the hexamer and drive conformational changes between subunits by altering the complementary hydrophilic protein-protein interfaces. Structural and biochemical analysis of five motifs in the protein suggest that ATP binding is a strained conformation recognized both by sensors and the Walker motifs and that intersubunit activation occurs by an arginine finger motif reminiscent of the GTPase-activating proteins. Taken together, these results provide insights into how RuvB functions as a motor for branch migration of Holliday junctions.

Keywords: AAA+-class ATPases; arginine finger; branch migration; Holliday junction; recombination

Introduction

Recombination is a general DNA repair pathway in eukaryotes and prokaryotes. Growing evidence suggests that one of the major functions of recombination is to restart replication forks that have been stalled due to DNA damage that may occur from 15% to 50% of the time, and may be more important in bacteria than the recombinational repair of double-stranded DNA (dsDNA) breaks.[1] The central, four-stranded recombination intermediate formed in both these repair processes is the Holliday junction, which can be generated by RecA and RecA homologs in dsDNA break repair[2] and in a RecA-independent fashion from replication forks.[3] Rapid migration of the Holliday junction in bacteria through heterologous DNA regions is performed by the RuvAB DNA translocase,[4–6] which is also implicated in the repair of stalled replication forks.[7]

The genes of the *ruv* locus operate late in recombination, and cells with mutations in these genes are sensitive to DNA damage, forming non-septate, multinucleate filaments that arise from covalently crosslinked chromosomes.[8] The RuvA protein forms symmetric tetramers and binds to one face of the Holliday junction.[9] The RuvB ATPase assembles into functional homohexameric rings and is the chemomechanical device that drives branch migration in the presence of RuvA.[10–11] The RuvC dimer resolves Holliday junctions by symmetrically nicking the Holliday junction at the crossover point. *In vivo* and *in vitro* data indicate that the RuvABC proteins function coordinately. RuvB, which has low affinity for Holliday junctions,[12–13]

Abbreviations used: dsDNA, double-stranded DNA; AAA, ATPases associated with diverse cellular activities; TIP49, TBP interaction protein of ~49 kDa; EM, electron microscopy; SAXS, small angle X-ray scattering; ss, single-stranded; PK, pyruvate kinase; LDH, lactate dehydrogenase.

E-mail address of the corresponding author: jat@scripps.edu

0022-2836/01/020297–14 $35.00/0

is targeted to opposite sides of the RuvA/Holliday junction complex through protein-protein interactions.[14] *In vivo*, RuvC functions only in the presence of RuvAB,[15] and can form a RuvABC/Holliday junction complex.[16] Thus, an RuvABC branch migration/resolution complex likely exists, similar to co-fractionating mammalian branch migration and resolution complexes.[17,18]

Structural studies of RuvB were undertaken to decipher the molecular basis for chemomechanical energy transduction and the mechanism of branch migration by the hexameric RuvB ATPases. Biochemical and structural studies of specific mutant RuvBs were pursued to probe specific mechanisms by which RuvB adopts different nucleotide-driven conformational changes. The RuvB structural results presented here provide insights into the structures of the archeal and eukaryotic TIP49 paralogs involved in chromatin remodeling and DNA repair.[19,20] Together, these results provide the framework for a detailed structural understanding of how RuvB converts chemical energy into the driving force behind branch migration of Holliday junctions formed during DNA recombination and DNA replication.

Results and Discussion

Structure of the RuvB subunit

Thermotoga maritima RuvB was crystallized in the space group $P6_5$ from active enzyme overexpressed in *Escherichia coli*,[21] and the structure of RuvB was determined to 1.6 Å resolution by multiple isomorphous replacement (Table 1). Electron density maps for the wild-type protein and the five active-site mutant structures were clear from Gln17 to Pro329, except for a disordered gap between Ile131 and Asp147. The RuvB subunit is made up of three sequential domains, which assemble into a fairly flat, triangular molecule ~25-35 Å thick and ~50 Å on each side (Figure 1(a)), and forms a helix with six subunits per turn through crystal packing. The N-terminal ATPase domain, domain I, represents about half of the protein and consists of a central five-stranded, all parallel β-sheet with the topology β5-β1-β4-β3-β2 that is surrounded by eight α-helices. The smaller, all-helical domain II (α9-11), and the mixed α-β C-terminal domain III (α13-17, β6-7), both pack against the C-terminal edges of the β-sheet of domain I. These three domains are linked by extended loops, which, although ordered in these crystal structures, could allow motion between the domains.

An ADP molecule binds at the interface of RuvB domains I and II (Figure 1(a)). The location of ADP within the RuvB structure immediately suggests that nucleotide binding states drive conformational changes between RuvB domains. Structural analysis and sequence conservation identify four motifs at the domain I-II boundary (Walker A, Walker B, sensor 1, and sensor 2) likely to be important in nucleotide-driven conformational changes of the

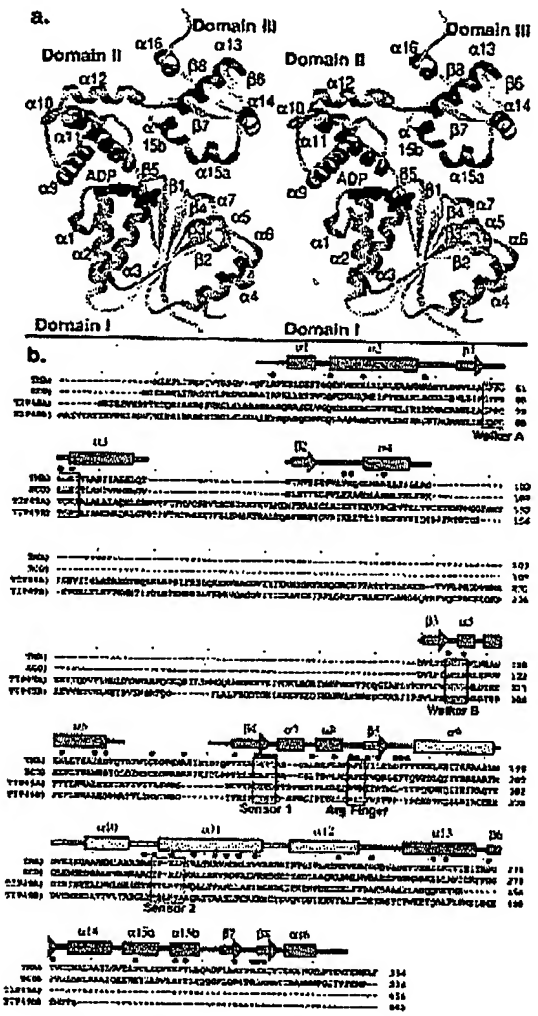

Figure 1. RuvB fold, domain assembly, functional motifs and ADP-binding position. (a) Each of the three RuvB structural domains is generated sequentially from the amino acid sequence, with an ADP molecule bound at the interface between the AAA+-class ATPase domains I (blue) and II (gold). The winged-helix domain III (green) is "masked" in these domain conformations, suggesting that DNA binding is induced only upon relative motion of the different domains. (b) Sequence alignment of *T. maritima* (TMA), *E. coli* (ECO) RuvB, *H. sapiens* TIP49a (TIP49A), and *H. sapiens* TIP49b (TIP49B) proteins displayed with the *T. maritima* secondary structure assignment. Gaps in the sequence are displayed as dashes. Red residues are absolutely conserved across an additional 15 different bacterial RuvB sequences. Red dots above the sequence represent strong and moderate dominant negative mutations isolated in the *E. coli* RuvB protein.[24] Sequence alignments were generated by the program SEQUOIA (CM Bruns, http://www.scripps.edu/~bruns/sequoia.html).

Table 1. *T. martima* RuvB crystallographic parameters and refinement statistics

Parameters	Native	Lys64Arg	Ala156Ser	Thr158Val	Arg170Ala	Pro216Gly		
Space group	$P6_5$	$P6_5$	$P6_5$	$P6_5$	$P6_5$	$P6_5$		
Beamline	SSRL 9-1	APS 14BMC	SSRL 9-1	ALS 5.0.2	SSRL 7-1	SSRL 7-1		
Wavelength (Å)	0.98	1.00	0.97	1.10	1.08	1.08		
Cell *a,b,c* (Å)	86.9, 86.9, 81.8	86.6, 86.6, 81.4	86.7, 86.7, 81.4	86.6, 86.6, 81.6	86.6, 86.6, 82.4	86.2, 86.2, 82.2		
Resolution (Å)	20-1.6/1.63-1.60	20-1.8/1.86-1.80	20-2.0/2.07-2.00	30-1.9/1.97-1.90	35-1.8/1.86-1.80	99-1.7/1.76-1.70		
Completeness (%)	99.0/99.0	89.5/79.8	99.1/91.4	99.2/97.6	97.4/83.5	98.1/94.8		
Reflections								
Observed	210,740	77,808	81,462	87,639	94,671	136,037		
Unique	45,763	29,025	23,654	26,948	31,816	37,484		
R_{sym} (%)[a]	7.1/46.0	5.8/36.6	7.7/41.0	3.6/12.8	5.7/49.0	4.4/33.2		
I/σ	29.4/3.1	23.8/2.7	18.4/3.4	23.8/8.2	17.1/1.5	27.0/2.6		
Mosaicity	0.7	1.4	0.4	0.3	0.2	0.4		
Refinement								
Resolution limits	20-1.6	20-1.8	20-2.0	20-1.9	20-1.9	20-1.7		
R_{cryst} (%)	23.4	23.4	21.6	22.6	21.6	22.0		
R_{free} (%)	25.3	26.6	25.0	24.9	25.0	25.6		
Parameters	$K_2Pt(CN)_4$	$K_2Pt(SCN)_4$	K_2AuBr_8	$AuCl_3$	K_2IrCl_6	K_2PtCl_6	K_2PtCl_4	SeMet
Concentration (mM)	1	1	1	1	1	1	0.1	-
Soaking time (hours)	4	1.5	21	2	24	6	2	-
Beamline	SSRL 9-1	SSRL 9-1	SSRL 9-1	SSRL 9-1	SSRL 9-1	SSRL 9-1	SSRL 9-1	SSRL 7-1
Wavelength (Å)	0.98	0.98	0.98	0.98	0.98	0.98	0.98	1.08
Resolution (Å)	1.8	2.0	2.9	3.2	2.1	2.0	2.3	1.95
Completeness (%)	99.6	100.0	95.7	99.1	99.5	100.0	99.4	98.2
Reflections								
Observed	201,526	181,430	22,701	24,777	83,921	313,379	47,868	62,398
Unique	32,506	23,865	7607	5773	20,532	23,775	15,438	25,243
R_{sym} (%)[a]	6.3	8.6	7.9	8.2	6.9	10.7	5.8	6.2
I/σ	33.4	34.6	16.4	25.9	25.1	37.1	22.0	16.2
Phasing[b]								
Number of sites	1	7	4	9	4	5	2	6
Resolution (Å)	2.5	2.5	2.5	3.2	2.5	2.5	2.5	2.5
R_{Cullis}								
Isomorphous	0.62	0.72	0.92	0.77	0.90	0.86	0.93	0.82
Anomalous	0.73	0.69	0.97	0.91	0.93	0.86	0.99	0.99
rms f/E_{iso}	1.12	1.57	0.72	1.39	0.75	0.95	0.65	1.11

[a] $R_{sym} = \Sigma_j |I_j - \langle I \rangle| \Sigma \langle I \rangle$ for all reflections (no σ cutoff).
[b] R_{Cullis}, rms f/E_{iso}, root-mean-square heavy atom F/isomorphous lack of closure error (phasing power).

protein structure (Figure 1(b)). The structures of domains I and II demonstrate that RuvB shares a common fold with the AAA+-super class of ATPases, named from an acronym of ATPases associated with diverse cellular activities.[22] The AAA+-class of ATPases includes chaperones, proteases, and nucleic acid processing enzymes, and has roles in vesicle fusion, vesicle formation, mitotic spindle formation and cytoskeletal integrity.

Domain III possesses the winged-helix DNA-binding fold, which is a modified form of the helix-turn-helix DNA-binding motif that is observed in many transcriptional regulators and in non-specific DNA-binding proteins such as histone H5 (reviewed by Gajiwala & Burley[23]). However, in the RuvB structure, the recognition helix α15, which lies in the DNA major groove in the canonical binding mode, is broken by the absolutely conserved Pro299 into α15a and α15b (Figure 1(a)). Extensive sequence conservation for domain III residues that possess both structural and potential recognition roles (Figure 1(b)) suggests the importance of this third domain, as does an isolated dominant negative nonsense mutation in *E. coli* RuvB[24] that preserves domains I and II, which pack into the hexamer, but deletes most of domain III.

This three-domain RuvB structure appears to be similar to the *Thermus thermophilus* RuvB structure recently published at 3.2 Å resolution determined independently[25] and a related *T. thermophilus* crystal form solved at 3.6 Å resolution (C.D.P. & J.A.T., unpublished results). This resemblance suggests that the high-resolution RuvB structure presented here is representative of all RuvB branch migration motors.

The RuvB structure furthermore rationalizes the insertions and deletions observed in the archaeal and eukaryotic RuvB homologs, termed TBP interaction protein of ~49 kDa (TIP49).[19,20] TIP49 proteins lack a RuvB-like domain III, but have a ~200 amino acid residue insertion between α3 and β3 (Figure 1(b)). This inserted domain appears to be unique to TIP49 by database searches and, given the ability of TIP49 to hexamerize, could be positioned where domain III sits in the RuvB structure near the C-terminal face of the domain I β-sheet. Thus, we suggest that the TIP49 inserted domain is positioned to function equivalently to RuvB domain III.

Implicated roles for Walker motifs A and B in RuvB conformational change

In addition to driving nucleotide triphosphate hydrolysis,[26] the RuvB structure suggests that conserved Walker A and B motifs may also function in driving conformational changes upon binding ATP. The Walker A motif, also termed the P-loop, is involved in coordination of the triphosphates and presenting the γ-phosphate group for cleavage. The Walker B motif coordinates a divalent metal ion and likely activates the water nucleophile for ATP cleavage. In the ADP-bound complex of RuvB (Figure 2(a)), the two motifs are not aligned appropriately for activating and cleaving ATP. This misalignment may also explain the inability to co-crystallize or soak divalent metals, non-hydrolyzable ATP analogs, or transition-state analogs such as aluminum and beryllium fluoride into this crystal form (data not shown), as these compounds would require a precise alignment of the active site.

Comparison of the Walker A and B motifs in these RuvB structures and in the AMP-PNP bound NSF-D2,[27,28] which possesses active-site geometry consistent with the highly conserved roles of Walker A and B in ATP hydrolysis, suggest that alignment of the motifs would result in local conformational changes that could be propagated into domain motions. Superposition of the central β-sheets in domain I suggests that ATP and/or metal binding may systematically shift α3 by ~3 Å towards the helical N terminus (Figure 3). Additionally, α2 would be shifted in the ATP state toward the protein core, partially accommodating the space left by α3. Combined, these motions would shift the orientation of domain II by ~30° at Walker A (Figure 3), and alter both the position of the winged-helix domain III and the subunit-subunit interface. Thus mutations in Walker A that disrupt normal γ-phosphate positioning, such as the Lys64Arg mutant (Figure 2(c)) whose guanidium group would likely shift the γ-phosphate group. The guanidium group position is constrained by other residues of Walker A (Gly58, Pro59, and Pro60), the β-sheet (Leu56, Ala57, Ala156, and Thr157), and the nucleotide and the conformational changes in both RuvB-like and NSF-D2-like conformations. Additionally, the residues of Walker B that inactivate the ATPase and branch migration activity[29] may impact both the hydrolytic machinery as well as an important sensor of the presence of a γ-phosphate group.

Although it is not possible to rule out that the RuvB/NSF-D2 differences are static variations in family members, the observed misalignment in the ADP-bound complex of RuvB is inconsistent with the conserved roles in an active ATPase site, which are supported by extensive mutagenesis for RuvB.[29,30] In the absence of direct superposition of the central β-sheet for these proteins, the most obvious marker for the misalignment becomes the relative distances between main-chain atoms for the Walker A and B motifs. In the NSF-D2 structure, the C^{α} atom for the Walker A lysine residue (Lys557 in 556-GKT-558) is roughly equidistant (~8.8 Å) from both of the C^{α} atoms of the Walker B carboxylate residues (Asp611 and Asp612 in 661-DDIE-614). For the RuvB structure, the C^{α} atom for the Walker A lysine residue (Lys64 in 63-GKT-65) is much closer to the C^{α} atom of the first carboxylate group (Asp109 at ~8.8 Å) than the second (Glu110 at ~10.7 Å). This difference is indicative of the systematic shift of α2 along the β-sheet and relates residues of Walker A that bind β and

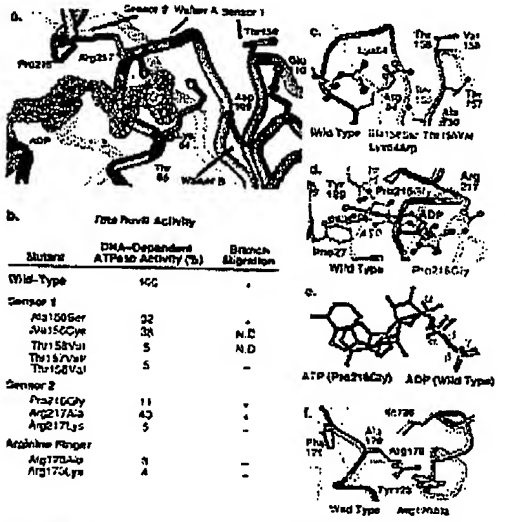

b.

Mutant	DNA-Dependent ATPase Activity (%)	Branch Migration
Wild-Type	100	+
Sensor 1		
Ala156Ser	32	+
Ala156Cys	38	N.D.
Thr158Val	5	N.D.
Thr158Val	5	–
Sensor 2		
Pro216Gly	11	+
Arg217Ala	43	+
Arg217Lys	5	–
Arginine Finger		
Arg170Ala	3	–
Arg170Lys	4	–

Figure 2. RuvB nucleotide recognition and an implied strained ATP-bound conformation. (a) Details of the nucleotide-binding site reveal that the phosphate groups are coordinated by the Walker A motif (including Lys64 and Thr65) with the ADP moiety contacted by residues of the sensor 2 motif (Pro216 and Arg217). Sensor 1 (Thr158) and Walker B (Asp109 and Glu110) motifs are located near the position of the γ-phosphate group. The isosurface of the simulated annealing omit difference density is shown for ADP, contoured at 3σ (green). (b) Structure-based mutational analysis reveals the importance of ATP hydrolysis in branch migration and the key roles played by sensor 1, sensor 2, and arginine finger in RuvB. Biochemical characterization of the DNA-dependent ATPase activity of RuvB mutants[21] and branch migration of an *in vitro* reconstituted RuvAB-Holliday junction complex.[51,52] Proteins scored as inactive, "–", in branch migration activity are either wholly or substantially compromised, as they showed less than 3% of wild-type activity after an incubation of 60 minutes. (c) Overlay of the wild-type RuvB protein (blue) with structures of the sensor 1 mutations Ala156Ser (yellow), Thr158Val (light blue), and the Walker A mutation Lys64Arg (light brown). (d) Overlay of the sensor 2 mutation Pro216Gly (yellow) with wild-type RuvB, illustrating some of the structural rearrangements required to accommodate the misregistered ATP (Figure 2(c)) in the nucleotide-binding site. (e) Details of ATP binding from the Pro216Gly structure (red) and ADP binding from the wild-type structure (blue) demonstrating the reorientation of the both adenine and ribose moieties and the phosphate misregistration, where the ATP γ-phosphate group binds at the β position and the ATP β-phosphate group binds at the α position. This structure suggests that binding ATP in the appropriate conformation channels binding energy into a strained RuvB conformation. (f) Overlay of the arginine finger mutation Arg170Ala (yellow) with wild-type RuvB, suggesting the dramatic loss of ATPase and branch migration assay are due to loss of the guanidium functionality, as structural perturbations are small.

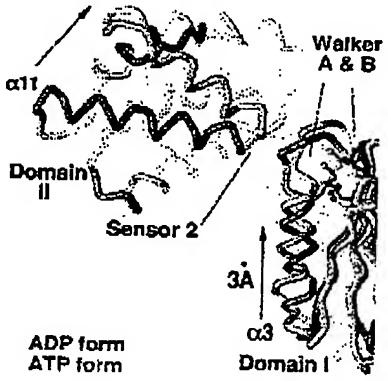

Figure 3. Nucleotide-driven conformational changes in AAA+-class ATPases. Overlay of the ADP bound RuvB domain I (blue) with the AMP-PNP bound NSF-D2 domain I (green) demonstrates the implied ~3 Å shift of α3 upon ATP binding, which aligns Walker A and B motifs (indicated by the conserved lysine residue of Walker A and carboxylate groups of Walker B), to generate an ATP hydrolysis site containing appropriate geometry as observed in NSF-D2. This motion of α3 is linked to a conformational change in domain II, in which the sensor 2 helix rotates dramatically. Comparison of the RuvB structure with other ADP-bound AAA+-class ATPases suggests that this structural rearrangement is the hallmark of this class of proteins.

γ-phosphate groups directly with the catalytic machinery at Walker B.

Roles for sensor motifs and evidence for a strained ATP state

From our RuvB structural and mutational results, we propose that RuvB exists in three distinct states with distinct conformational states during the reaction cycle: ATP-bound, ADP-bound, and empty. Recognition of each of these states is likely *via* two types of detectors that interact either with the ADP moiety or with the ATP γ-phosphate group. In addition to the interaction of the Walker A and B motifs in sensing the ATP-bound state, the sensor 1 and sensor 2 motifs are critical for responding to the nucleotide based on both structural analysis and mutagenesis results (Figure 2(a)-(c)).

Sensor 1 is located on domain I at β4 between the Walker A and B motifs (Figure 2(a)), and appears positioned to distinguish nucleotide diphosphate and triphosphate states by forming a hydrogen bond through the Thr158 side-chain to the ATP γ-phosphate group. The Thr158 side-chain, even when rotated about χ1, is not close enough to form a hydrogen bond to a modeled γ-phosphate group (5.5 Å) in this ADP-complex structure (Figure 2(b)); however, the proposed shift of Walker A and B motifs in response to ATP

binding would bring the Thr158 side-chain into position (~3 Å) for hydrogen bond formation. Significantly, mutation of Thr158 to the isosteric valine inactivates DNA-dependent ATPase activity (Figure 2(b)), even though the mutation does not change the structure of the ADP-bound form of the enzyme (Figure 2(c)). The other absolutely conserved residues in the sensor 1 motif do not appear to sense the ATP state of the enzyme directly, but likely play structural roles. Gly155 packs directly against the hydrophobic core of the protein, and any other residue would possess substantial steric clashes. Ala156 lies underneath Walker A, and residues with large side-chains would disrupt the position of Lys64. Mutation of Ala156 to either serine or cysteine is tolerated (Figure 2(b)), and the structure of the Ala156Ser mutant is undisrupted in the ADP-bound complex (Figure 2(c)); however, this position is strictly conserved as alanine in all bacterial RuvB sequences and could be more problematic, depending on the structural influence of ATP or DNA-dependent rearrangements on this region. Thus, sensor 1 may help distinguish between nucleotide diphosphate and nucleotide triphosphate-bound states of the enzyme.

Sensor 2, located on domain II (Figure 2(a)), packs against the ATPase binding site. Pro216, which is conserved in RuvBs as either proline or methionine, packs directly against the adenine face, and Arg217 forms a charged hydrogen bond to the β-phosphate group. Mutations in both of these sensor 2 residues affects the ATPase activity of the enzyme. The mutation of Arg217 to lysine inhibits ATPase activity, although the Arg217Ala mutant activity is higher (Figure 2(b)). Mutation of Pro216 to glycine shows hindered ATPase activity at low enzyme concentrations (data not shown), but normal ATPase activity at high concentrations (Figure 2(b)). Notably, the crystal structure of this mutant (Figure 2(d)–(e)) reveals that Pro216 is important for preventing alternative nucleotide-binding states from occurring. Thus, the Pro216Gly mutant surprisingly binds ATP, not ADP, as isolated from cells, but the ATP binds non-productively, such that the phosphate groups of the ATP are out of register. The ATP γ-phosphate group binds in the normal β position and the ATP β-phosphate group binds in the normal α position (Figure 2(e)). This out-of-register binding is accommodated by a rearrangement of the binding site that is prevented in the wild-type protein by steric collision between the nucleotide 3′ hydroxyl group and the Pro216 ring. The ADP molecule bound by the wild-type enzyme is in the *anti* conformation, while the ATP molecule in the Pro216Gly is *syn*. Importantly, the altered nucleotide-binding mode in this mutant and its inefficiency at lower protein concentrations suggests that correct positioning of the ATP γ-phosphate group is energetically costly, consistent with the γ-phosphate-induced conformational changes inferred from the structure. Both Pro216 and Arg217 in sensor 2 interact with components of the nucleotide present in both ADP and ATP. Hence, this motif, unlike sensor 1, likely distinguishes between nucleotide-bound and unbound states in addition to enforcing a strained ATP-bound conformational state to prevent non-productive binding.

Although the sensor 2 motif was previously defined only for the highly conserved region,[31] analysis of the RuvB structure suggests that the motif definition should be expanded. The adenosine ring is buried within a pocket and sequestered from solvent by the hydrophobic side-chains of Pro21, Phe27, Ile188, and Pro216. This hydrophobic collapse can be likened to a vise in which domains I and II clamp down on the flat adenine. The polar faces of the ring interact with more polar environments: N-1 and N-3 hydrogen bond to water molecules; the exocyclic N-6 amine hydrogen atom bonds to the Ile28 backbone carbonyl group; and N-7 is oriented towards the Tyr180 hydroxyl and Leu62 backbone carbonyl groups. The ADP 2′ and 3′-hydroxyl groups make no specific protein interactions, and the only specific hydrogen bonding interaction with ADP is through the exocyclic amine group. This lack of specific interactions explains the ability of the *E. coli* and *T. thermophilus* RuvBs to utilize alternative nucleotides including dATP, dCTP, and dTTP.[13,32] The possibility that the more hydrophilic guanine base may prevent the hydrophobic collapse between domains I and II may explain biochemical studies for the *Thermus* RuvB that can hydrolyze GTP and dGTP efficiently, but cannot use these nucleotides for *in vitro* branch migration,[32] as nucleotide binding is decoupled from the hydrophobic collapse.

All three states of the enzyme can be detected through recognition of either the ADP moiety or the γ-phosphate group. The sensor 1 and the Walker A and B motifs respond to the binding of the γ-phosphate group and a divalent cation. This ATP state, as revealed by the alternative nucleotide binding in the Pro216Gly mutant, is likely to exist in a tense or strained conformation with a triggered structural transition (Figure 3). Sensor 2 recognizes the ADP through interaction with the sugar and diphosphate moieties as well as hydrophobic collapse around the ring. These three RuvB conformational states within domains of an individual RuvB subunit provide the chemomechanical force that drives Holliday junction branch migration in the context of an active hexamer.

RuvB hexameric assembly

The crystallographically determined subunit contacts in the helix with six subunits per turn use the same molecular interfaces that are observed in the HslU and NSF-D2 hexameric AAA+-class ATPases.[27,28,33,34] Superimposition of RuvB domain I onto the conserved domain of HslU results in a polar hexamer (Figure 4(a)) that satisfies known constraints, including the two-lobe construction (the large lobe is domains I and II, the small lobe is domain III) and dimensions observed by electron

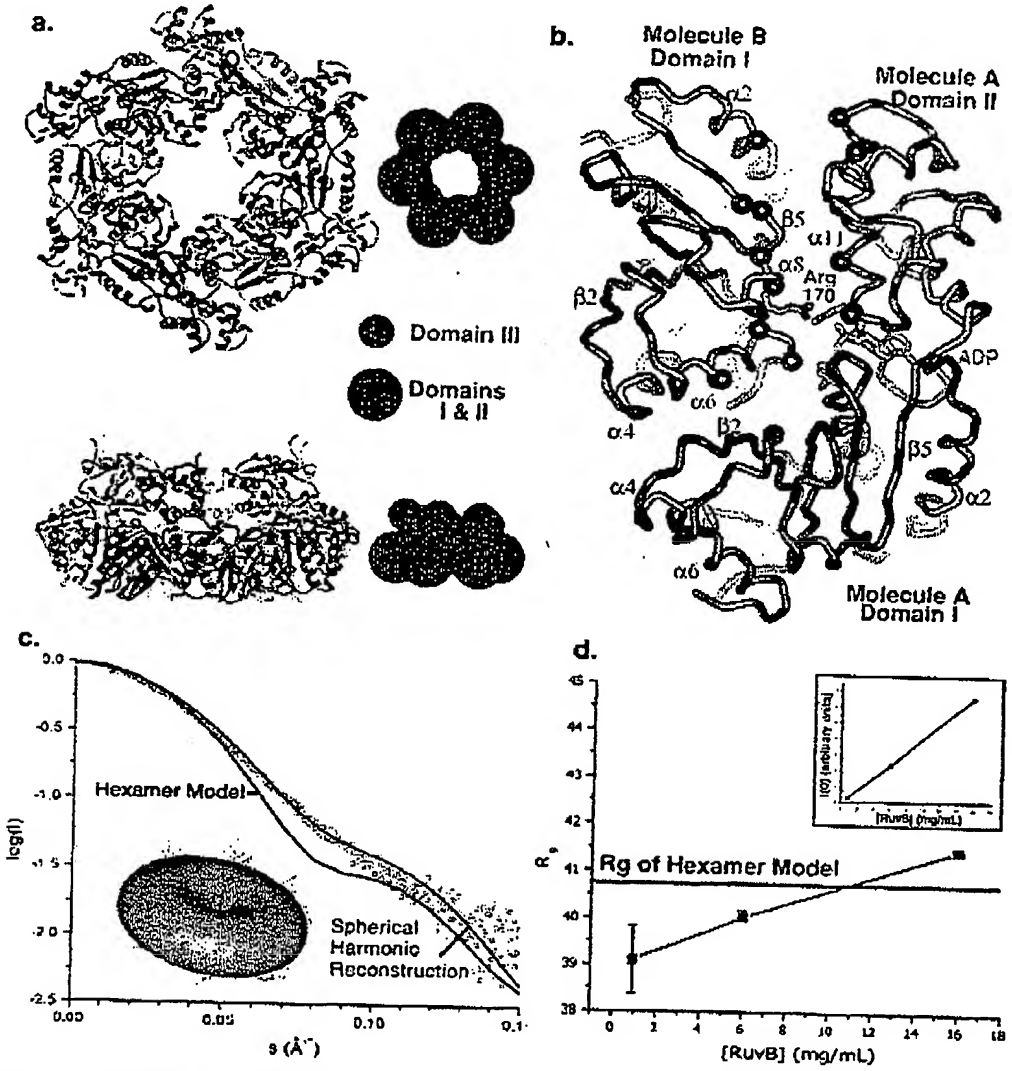

Figure 4. RuvB hexameric interfaces and assembly. (a) The RuvB hexamer assembly generated from the HslU hexamer (PDB code 1DO0[34]) closely resembles EM reconstructions of RuvB hexamers bound to DNA.[35] The large lobe of the polar ring is generated from domains I and II, while the small lobe comprises domain III. (b) Hexameric interface between two adjacent subunits of the RuvB hexamer. The hexameric interface is assembled entirely from domains I and II. Dominant negative mutations[24] along these interfaces are indicated by a red sphere at the amino acid C^{α} position. The side-chain of the arginine finger (green) of molecule B approaches the bound nucleotide (yellow) within the adjacent molecule A. (c) Fit of the *Thermotoga* RuvB hexamer assembly (blue) and a spherical harmonic reconstruction (green) to SAXS data collected from *E. coli* RuvB hexamers at 6 mg/ml. The spherical harmonic reconstruction shown here ($L = 2$, $p3$ symmetry) is representative of the flattened toroids generated *ab initio* from the experimental data. (d) The calculated hexamer radius of gyration (R_g) closely matches the experimentally determined values. Importantly, the forward scattering intensity ($I(0)$) is linear in response to RuvB concentration, indicating that aggregation and hexamer disassembly were not occuring during these SAXS measurements.

microscopy (EM).[35] The entire subunit interface, made up almost entirely by domains I and II, is hydrophilic and possesses extensive shape complementarity (Figure 4(b)). The domain I-domain I interface between adjacent subunits is slightly negatively charged, whereas the domain I-domain II interface is positively charged. The binding of domain I within the cleft formed by domains I and

II of the adjacent subunit (Figure 4(b)) provides a mechanism whereby nucleotide-induced conformational changes between domains I and II can affect the subunit-subunit interactions (Figure 3) and suggest that subunits shift positions during the reaction cycle.

This assembly is also consistent with our experimental small-angle X-ray scattering (SAXS) data measured on solutions of *E. coli* RuvB hexamers (Figure 4(c)). Calculated scattering from the hexamer is similar to the experimental scattering curve (Figure 4(c)). SAXS data provide an overall radius of gyration (R_g) for the particle of ~40 Å (Figure 4(d)) with a maximum intraparticle distance (D_{max}) of ~120 Å, consistent with our hexamer model (Figure 4(d)). Additionally, an *ab initio* spherical harmonic reconstruction, which fits the experimental curve with a small number of parameters,[36] agrees fairly well with the hexamer (Figure 4(c)). SAXS data can exclude packing arrangements that give different radii of gyration and maximum interparticle distances, such as more globular arrangements or asymmetric hexamers that are more elliptical and would have increased maximum intraparticle distances. SAXS cannot provide atomic-resolution details of the interfaces of this prolate ellipsoid model as shown through systematic generation of 64,000 computational perturbations of this hexamer (data not shown); however, there is no reason *a priori* to expect that any computationally generated assembly should be in agreement with these experimental SAXS data. Taken together, the agreement of the hexamer with experimentally determined SAXS data, the similarities to EM reconstructions,[35] the conservation with other hexameric AAA + -class ATPases,[27,28,33,34] and similarities to the crystallographic packing interfaces suggest that this hexamer arrangement is likely to be correct.

Assembly is critical for ATPase activity in RuvB[37,38] and in other AAA + -class ATPases.[22] RuvB is known to be functional as a hexamer and assemble into rings.[35] The fact that ADP-bound RuvB assembles into a helix with six subunits per turn in these crystals rather than a hexameric ring suggests that asymmetry in the RuvB ring arises simply through assembly and that not all subunits of a hexameric ring can exist in an ADP-bound form. Both the RecA and T7gp4 proteins have been observed in helical and ring forms, and these proteins are believed to possess functional asymmetries.[39,40]

Arginine fingers in AAA+-class ATPases

To test the role of the strictly conserved arginine following the Walker A and B motifs in functional hexameric AAA + -class ATPases, Arg170 in RuvB was mutagenized to both alanine and lysine. Both mutants were deficient ATPases and were not activated upon DNA binding like wild-type (Figure 2(b)). These results match the inactivation observed in mutants of the equivalent arginine to leucine and lysine in the AAA + -class ATPase domain of the *E. coli* FtsH ATPase-dependent protease[41] and an arginine to histidine mutation isolated in *E. coli* RuvB.[24] The crystal structure of Arg170Ala lacks any real conformational changes from wild-type (Figure 2(f)), indicating that the defect in the mutant involves loss of the arginine guanidium group.

The hexameric assembly demonstrates that the arginine residue approaches the nucleotide phosphate groups (Figure 4(b)) and may function analogously to arginine fingers identified in the GTPase-activating proteins (GAPs). These arginine residues function to regulate nucleotide hydrolysis by binding the γ-phosphate group within the Ras GTPase switch, which activates GTPase activity by 10^5-fold (reviewed by Noel[42]). Arginine fingers have been implicated in a number of other unrelated NTPases, including Rho GTPases,[43] T7gp4,[40] and F_1-ATPase.[44] In the RuvB hexamer, Arg170 deviates slightly from the position required to facilitate ATP hydrolysis (Figure 4(b)), suggesting that ADP-bound RuvB is not the correct state to activate ATP hydrolysis in the adjacent subunit. In fact, proper arginine geometry for ATP hydrolysis can be observed by modeling in NSF-D2 bound to the non-hydrolyzable ATP analog AMP-PNP,[43] suggesting that ATP binding in one subunit drives ATP hydrolysis in the adjacent molecule. These structural and biochemical results provide a mechanism to explain previous kinetic proposals[38,45] in which ATP is both a substrate and an allosteric effector.

Model for the RuvABC complex

Double-stranded DNA can pass through the center of the RuvB hexamer (Figure 5(a)) that ranges from 25 to 35 Å in diameter. This is in contrast to the unrelated phage T7 gp4 hexameric DNA helicases, where unwinding is believed to be driven by translocation of only a single strand through the center,[40] and would explain why RuvB can translocate along DNA[37] but fails to act as a helicase in the absence of RuvA.[10] Biochemical data also support both strands passing through the center of the hexamer. RuvB appears to be able to migrate through interstrand psoralen crosslinks,[46] and protects about 24 base-pairs of both DNA strands in DNase I footprinting experiments.[47] The 1.5 turns of *B*-DNA within the central channel of the hexamer (Figure 5(a)) are also consistent with the geometry of the RuvA/Holliday junction complex[9] and closely resemble EM reconstructions of RuvB bound to plasmid DNA[35] in which DNA is bound at either end of the hexamer (domain I and domain III) surrounding an interior cavity (the gap between domain II and DNA).

Domain III of RuvB overlays well with other winged-helix domains (Figure 5(b)). Two different DNA-binding modes have been observed for this family of proteins;[23] however, both involve faces of domain III that are not oriented towards the DNA

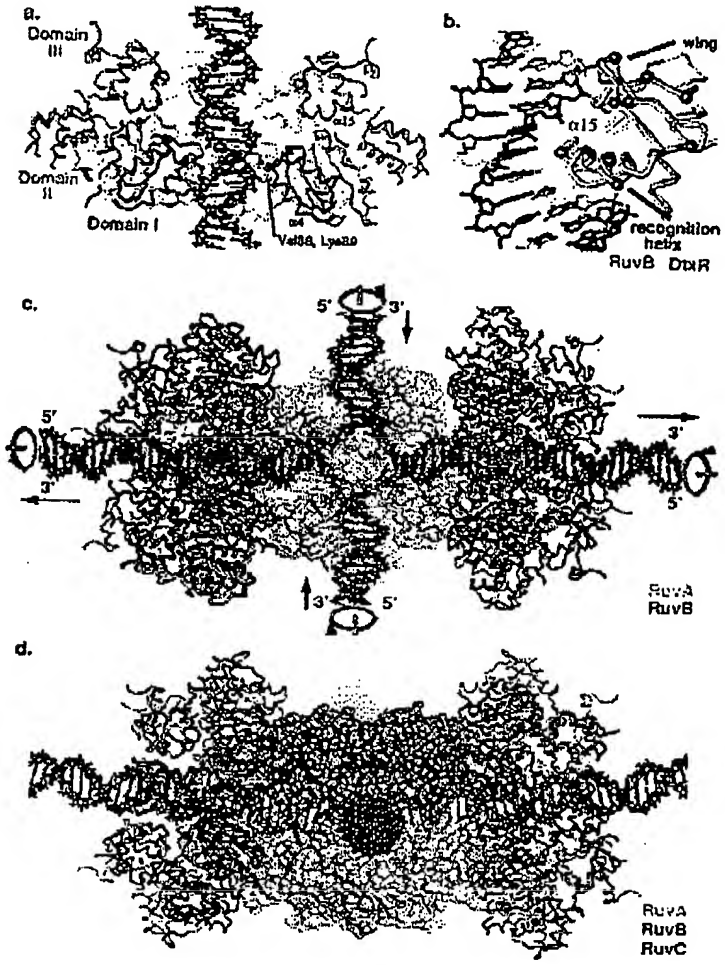

Figure 5. Structurally implied RuvB/DNA and RuvABC/Holliday junction interactions. (a) The structurally implied path of duplex DNA through the RuvB hexamer in Holliday junction branch migration. Domains I (blue) and III (green) are positioned to interact with the DNA (black). The β2-α4 loop forms a tight constriction around the DNA and includes Val88 and Lys89, identified as positions of dominant negative mutations in *E. coli* RuvB,[38] and shown as red balls as are similar mutations in domain III. Topological evidence suggesting that the DNA is melted or underwound[21,38,49] is not illustrated here. (b) Superposition of the domain III of RuvB (green) onto the diphtheria toxin repressor (DtxR)-DNA co-crystal structure (purple, PDB code 1DDN[61]). The DtxR utilizes the canonical mode for winged helix binding in which the recognition helix (α15a and α15b in RuvB) lies in the major groove and the wing contacts DNA phosphate groups. This canonical binding mode[23] is most consistent with the positive charge of the wing and net negative charge of the recognition helix. Cα positions of residues critical for RuvB function in this domain[24] are indicated by red balls and, excluding residues involved in the stabilization of the domain, include the positive charges and glycine of the wing and residues of the recognition helix that contact the DNA major groove. Placing this face of the domain against DNA running through the hexamer (a) requires a 60-90° rotation of domain III relative to the AAA+-class ATPase domains I and II. (c) Depiction of the RuvAB/Holliday junction complex shows the RuvB hexamers (dark blue, purple) on either face of the RuvA tetramer (yellow surface, PDB code 1BDX[9]). The orientation of the RuvB hexamer is derived from EM images indicating that the large lobe (domains I and II) face the RuvA hexamer.[14] The rings are rotated so that domain III from one of the RuvB subunits is aligned with the DNA major groove, as suggested by the winged-helix binding mode, and the rings are related by a 2-fold rotation about an axis perpendicular to the page. The direction of the DNA migration and rotation is indicated by arrows in which two duplexes (red and blue) are unwound and recombined in the RuvA tetramer. (d) Depiction of the RuvABC/Holliday junction complex rotated 90° relative to (a) showing the binding of the RuvC dimer to the face of the Holliday junction opposite RuvA. The RuvC dimer (red surface, PDB code 1HJR[62]) is oriented so that the active sites face the phosphodiester backbone and the fit suggests that RuvC should make protein-protein contacts with RuvB, as suggested from biochemical results.[16]

in the hexamer assembly of ADP-bound conformations of RuvB (Figure 5(a)). Thus, unless domain III of RuvB possesses a third, novel binding mode, this domain needs to be reoriented by 60-90° to present the appropriate binding face towards the DNA passing through the central channel of the complex. A canonical winged-helix interaction is supported by both homology and dominant negative mutations (Figure 5(b)), the flexible random-coil linkage between domains II and III, and a ~20° rotation of domain III relative to domains I and II determined by superimposing the *T. maritima* RuvB structure and the *T. thermophilus* RuvB structures ([25]; C.D.P. & J.A.T., unpublished results). If the rearrangement occurs, appropriate domain III orientations may be forced by packing interaction between adjacent domain IIIs that does not occur in the crystal packing.

An ATP-bound state of RuvB modeled from NSF-D2 (Figure 3) would force domain III into closer proximity to DNA, consistent with both gel shift experiments[48] and DNase I footprints in which ATPγS improves the protection of the domain III side of the footprint.[47] Winged-helix domains have been structurally characterized only with dsDNA, and the RuvB structure suggests that RuvB may interact primarily with and translocate along both strands of dsDNA. Paradoxically, the helicase activity of RuvAB possesses a 5′ → 3′ directionality,[10] but has not been characterized independently of RuvA. The resolution of this problem may be that strand specificity in the *in vitro* helicase reaction may be due to differences in the way RuvA presents 5′ and 3′-tailed substrates to the RuvB translocase and not to strand specificity of RuvB itself.

The large face of the RuvB hexamer faces the RuvA tetramer[14] and can be associated with domains I and II from these crystallographic results (Figure 5(c)). This orientation of the RuvB ring places the disordered region between Ile131 and Asp147 onto the RuvA contact region, which forms a crystal contact as a pair of interacting β-hairpins in the *T. thermophilus* crystal form[25] (C.D.P. & J.A.T., unpublished results). Geometric constraints demand that only one or two RuvB subunits interact with the RuvA tetramer at any one time. Interestingly, the RuvB subunit positioned to place the winged-helix domain into the DNA major groove is also the subunit positioned to interact with RuvA. An RuvC dimer fits in the RuvAB/Holliday junction complex (Figure 5(d)) such that the active sites can generate two symmetrical cuts, consistent with genetic and biochemical data indicating that RuvC functions in concert with RuvAB.[15,16]

Structural implications for RuvB-driven DNA translocation and branch migration

Branch migration by the RuvAB complex requires a screw motion of the DNA (Figure 5(c)), which includes both translational and rotational components. The result of this motion is to change the identity of the bases being migrated through a DNA pathway defined by the backbone, but not to move the pathway itself. This restriction makes any proposed RuvAB mechanism different from the proposed single-stranded (ss)DNA migration models in T7gp4, in which simple translation of the DNA can occur along with motion of the backbone positions.[10] Two classes of different, testable models can be proposed for branch migration by RuvAB, both of which are influenced dramatically by the fixed nature of the backbone pathway and cannot be distinguished by current experimental evidence.

The first class of models would involve a fixed RuvAB interaction, in which RuvB molecules remain fixed to RuvA once the complex is formed. In this class of models, only one or two subunits will be in the correct position to perform work during the branch migration reaction due to the fixed DNA backbone pathway. In this scenario, the arginine finger motif may function to prevent wasteful ATP hydrolysis prior to multimer assembly or trigger ATP hydrolysis in the active subunit once conformational changes due to ATP binding have occurred. The topological distortions observed for trapped RuvB-DNA complexes[21,38,49] may arise from distortions in the ATP-bound state of RuvB that are unable to relax without ATP hydrolysis.

The second class of models would provide for a rotating RuvAB interaction, in which RuvB molecules rotate into and out of the active position in response to ATP hydrolysis (Figure 6). Rotation of the RuvB hexamer relative to RuvA could be driven both by interaction with the DNA template and the nature of the RuvAB interface itself. This

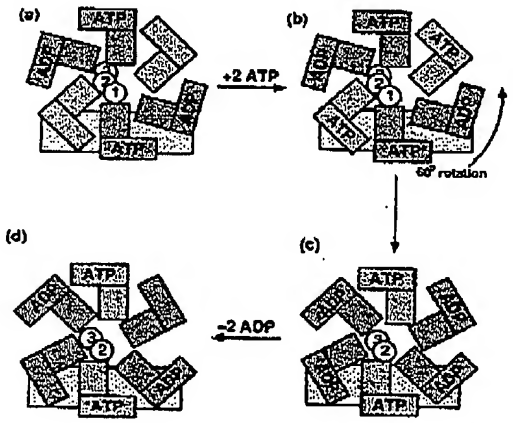

Figure 6. Structurally implied mechanism for branch migration. Illustration of a mechanism for RuvB branch migration involving a rotation of the RuvB hexamer (green, cyan, and blue subunits) relative to the RuvA tetramer (yellow bar). Stepwise migration of the DNA is indicated by motion of the circled numbers through the center of the hexamer, although the fundamental translocation step size is unknown. The 2-fold symmetry of the loading of the nucleotide binding sites is based on pre-steady state kinetics of RuvB, which hydrolyzes two ATP molecules per hexamer.[38,45] The starting state (a) with two ATP and two ADP molecules is inferred from the optimal nucleotide ratio (2 ATPγS:1 ATP) for forming topologically underwound DNA,[21,38,49] equivalent to step (b), and the productive arginine finger geometry observed in the AMP-PNP bound NSF-D2.[41] ATP hydrolysis in step (b) may drive rotation of the RuvB hexamer (c) by opening of the ADP-bound state along DNA as well as through interactions with RuvA. ATP serves as an allosteric effector for ADP release,[45] which may be driven by interface changes between subunits that may be released after rotation (d) or during rotation. Hydrolysis of ATP by RuvB is kinetically rapid and ADP release is slow.[45]

model is also consistent with biochemical data suggesting ATP is both substrate and allosteric effector,[38,45] inducing ADP release in other binding sites, likely due to the influence of ATP-induced domain I-II changes upon the hexamer interface (Figure 4(b)). The orientation of the arginine finger, which likely triggers hydrolysis in the ATP bound form, would be consistent with the required counter-clockwise screwing of DNA through the RuvAB complex (Figure 6). Topological distortions for trapped RuvB-DNA complexes may be due to a symmetry mismatch between the hexameric RuvB ring (60° steps from the six subunits) and DNA (36° steps from the ten base-pairs per turn).

For the rotating RuvAB interaction, RuvA may function as an adenine nucleotide exchange factor, driving ADP/ATP exchange in the bound RuvB molecule and driving RuvB rotation once ATP is hydrolyzed. RuvA improves the ATPase activity of RuvB with and without DNA,[45] increasing the K_m of RuvB for ATP by seven to eight-fold and maximizing the hydrolysis rate at an 8:6 RuvA:RuvB stoichiometry, which is the maximum number of tetramers that can sterically interact with one face of a RuvB hexamer. The isolated C-terminal RuvA domain that binds RuvB inhibits ATP hydrolysis,[50] possibly representing a state in which each RuvB subunit remains bound to a RuvA domain and ATP.

These structural and mutagenesis studies of RuvB suggest in detail how RuvB utilizes the AAA+-class ATPase fold to convert nucleotide binding and hydrolysis to mechanical action in the migration of Holliday junctions. The structural results strongly suggest that domain-domain motions triggered by nucleotide-bound states drives the hexamer subunit-subunit conformational changes. Additionally, the helix formed by the ADP-bound RuvB strongly suggests that asymmetry is key to function of the hexamer, and the arginine finger provides a mechanism to couple sequential hydrolysis between adjacent subunits potentially producing a wave of ATP hydrolysis in the ring. These results can be interpreted in terms of either rotating or fixed RuvAB translocation models, neither of which is clearly distinguishable with current data. These results provide a framework to experimentally address a number of important questions regarding RuvB function, including determination of the step size and the number of nucleotides hydrolyzed per step, elucidation of the atomic structure and the permanency of the RuvAB interaction, and delineation of the functionally relevant nucleotide-loaded states of the hexamer during branch migration.

Experimental Procedures

RuvB expression, mutagenesis, and biochemical characterization

T. maritima RuvB was overexpressed recombinantly in *E. coli* and purified as described.[21] The selenomethionine-incorporated protein was generated by cloning the RuvB expression plasmid into methionine auxotrophic *E. coli* strain B834 (Novagen) followed by expressing in LeMaster's defined medium with methionine replaced with 50 mg/l of D,L-selenomethionine (Sigma). *T. maritima* RuvB mutants were generated performing the QuickChange PCR protocol (Stratagene) on the pET11c expression construct.[21]

RuvB DNA-dependent ATPase activities were measured using a colorimetric assay that detected the release of inorganic phosphate[21] using 5-20 μg of protein per reaction. Branch migration assays utilized *T. maritima* RuvA and Holliday junctions prepared as described.[51,52] Briefly, Holliday junction arms were generated using PCR snapback products and these arms were then annealed at 70 °C. Products of RuvAB branch migration for these substrates are heteroduplexes. Importantly, use of mismatches in the Holliday junctions forces the reaction to be energetically disfavored, preventing thermally driven migration of the junctions. Reactions were analyzed using native polyacrylamide gels and were stained with ethidium bromide.

Crystallization and X-ray structure determination

Crystals of RuvB were grown by vapor diffusion in sitting drop plates against 1 M 1,6-hexanediol, 100 mM $CoCl_2$, 100 mM sodium acetate (pH 4.6). Crystals were cryocooled in mother liquor supplemented with 20% (w/v) glycerol. X-ray diffraction data were collected at the Stanford Synchrotron Radiation Laboratory (SSRL), the Advanced Light Source (ALS), and the Advanced Photon Source (APS). Data were processed using Denzo and Scalepack.[53]

One strong initial $K_2Pt(CN)_4$ site was identified through isomorphous and anomalous Pattersons, and other derivative sites were subsequently identified by cross-phasing. Protein phases were generated with MLPHARE in the CCP4 package,[54] and an initial structure was built with Xfit.[55] Refinement was performed with CNS version 1.0[56] by using the maximum-likelihood target function with 10% of the reflections omitted from the refinement for cross-validation testing[57] with manual inspection and rebuilding into σA-weighted $2F_{obs} - F_{calc}$ and $F_{obs} - F_{calc}$ electron density maps with Xfit. The methionine positions of the refined structure were verified through isomorphous difference Fourier maps calculated by using data from the selenomethionine-substituted protein (data not shown).

Identification of ADP in the crystal structure

ADP was identified by examination of the bound nucleotide density and verified with a standard ATP regeneration system in which ATP formation from ADP is linked to NADH oxidation with pyruvate kinase (PK) and lactate dehydrogenase (LDH) and measured spectrophotometrically ($\Sigma_{340} = 6.22\ cm^{-1}\ mM^{-1}$). Typical reaction conditions contained the following: 5 mg of acid-denatured RuvB, 1 mM phosphoenolpyruvate, 250 μM NADH, 20 units of LDH/ml, 40 units of PK/ml, and 5 mM DTT in 200 mM Hepes (pH 7.5). Data from the assay indicate that ~50% of the purified protein was bound to ADP (data not shown).

Small-angle X-ray solution scattering

E. coli RuvB was expressed from the pEAW112 plasmid and isolated by using published protocols.[5] Hexamers were formed by concentration and isolated by gel filtration on a Superose-12 column in 20 mM Tris-HCl (pH 8.0), 50 mM NaCl, 1 mM DTT. Scattering data were collected at the SSRL beamline 4-2. For each concentration, the Guinier region of the small-angle scattering was linear. R_g, D_{max} and $I(0)$ were derived from experimental data using GNOM.[58] Spherical harmonic reconstructions were generated using SASHA[56,59] and fits of the computational hexamers were calculated through CRYSOL.[60]

Protein Data Bank accession numbers

Coordinates for native RuvB and the Lys64Arg, Ala156Ser, Thr158Val, Arg170Ala, and Pro216Gly mutants have been deposited in the RCSB Protein Data Bank under the entries 1IN4, 1IN6, 1IN5, 1IN8, 1IN7, and 1J7 K, respectively.

Acknowledgments

We thank Karl-Peter Hopfner and Clifford Mol for helpful discussions; Clifford Mol, David Barondeau, and Andrew Arvai for assisting data collection; and Jie Tong for purifying samples of RuvB that initiated the crystallographic efforts. We are indebted to Tom Macke for the computational generation DNA coordinates for Figure 5. We thank the staff at the crystallographic beamlines at SSRL, ALS, and APS for excellent data collection facilities. The pEAW112 plasmid was a kind gift from Michael Cox. This work is based upon research conducted at the Stanford Synchrotron Radiation Laboratory (SSRL), which is funded by the Department of Energy (BES, BER) and the National Institutes of Health (NCRR, NIGMS), the Advanced Light Source (ALS) at Lawrence Berkeley National Laboratory (LBNL), and the Advanced Photon Source (APS) at the Argonne National Laboratory. This work has been funded by the NIH grant CA76431 to J.A.T. and a Howard Hughes Predoctoral Fellowship to C.D.P.

References

1. Cox, M. M., Goodman, M. F., Kreuzer, K. N., Sherratt, D. J., Sandler, S. J. & Marians, K. J. (2000). The importance of repairing stalled replication forks. *Nature*, 404, 37-41.
2. Cox, M. M. (1999). Recombinational DNA repair in bacteria and the RecA protein. *Prog. Nucl. Acid Res. Mol. Biol.* 63, 311-366.
3. Zou, H. & Rothstein, R. (1997). Holliday junctions accumulate in replication mutants via a RecA homolog-independent mechanism. *Cell*, 90, 87-96.
4. Iype, L. E., Inman, R. B. & Cox, M. M. (1995). Blocked RecA protein-mediated DNA strand exchange reactions are reversed by the RuvA and RuvB proteins. *J. Biol. Chem.* 270, 19473-19480.
5. Iype, L. E., Wood, E. A., Inman, R. B. & Cox, M. M. (1994). RuvA and RuvB proteins facilitate the bypass of heterologous DNA insertions during RecA protein-mediated DNA strand exchange. *J. Biol. Chem.* 269, 24967-24978.
6. Adams, D. E. & West, S. C. (1996). Bypass of DNA heterologies during RuvAB-mediated three- and four-strand branch migration. *J. Mol. Biol.* 263, 582-596.
7. Seigneur, M., Bidnenko, V., Ehrlich, S. D. & Michel, B. (1998). RuvAB acts at arrested replication forks. *Cell*, 95, 419-430.
8. Ishioka, K., Fukuoh, A., Iwasaki, H., Nakata, A. & Shinagawa, H. (1998). Abortive recombination in *Escherichia coli ruv* mutants blocks chromosome partitioning. *Genes Cells*, 3, 209-220.
9. Hargreaves, D., Rice, D. W., Sedelnikova, S. E., Artymiuk, P. J., Lloyd, R. G. & Rafferty, J. B. (1998). Crystal structure of *E. coli* RuvA with bound DNA Holliday junction at 6 Å resolution. *Nature Struct. Biol.* 5, 441-446.
10. Tsaneva, I. R., Muller, B. & West, S. C. (1993). RuvA and RuvB proteins of *Escherichia coli* exhibit DNA helicase activity *in vitro*. *Proc. Natl Acad. Sci. USA*, 90, 1315-1319.
11. Muller, B., Tsaneva, I. R. & West, S. C. (1993). Branch migration of Holliday junctions promoted by the *Escherichia coli* RuvA and RuvB proteins. I. Comparison of RuvAB- and RuvB-mediated reactions. *J. Biol. Chem.* 268, 17179-17184.
12. Tsaneva, I. R. & West, S. C. (1994). Targeted versus non-targeted DNA helicase activity of the RuvA and RuvB proteins of *Escherichia coli*. *J. Biol. Chem.* 269, 26552-26558.
13. Parsons, C. A. & West, S. C. (1993). Formation of a RuvAB-Holliday junction complex *in vitro*. *J. Mol. Biol.* 232, 397-405.
14. Yu, X., West, S. C. & Egelman, E. H. (1997). Structure and subunit composition of the RuvAB-Holliday junction complex. *J. Mol. Biol.* 266, 217-222.
15. Mahdi, A. A., Sharples, G. J., Mandal, T. N. & Lloyd, R. G. (1996). Holliday junction resolvases encoded by homologous *rusA* genes in *Escherichia coli* K-12 and phage 82. *J. Mol. Biol.* 257, 561-573.
16. Davies, A. A. & West, S. C. (1998). Formation of RuvABC-Holliday junction complexes *in vitro*. *Curr. Biol.* 8, 725-727.
17. Constantinou, A., Davies, A. A. & West, S. C. (2001). Branch migration and Holliday junction resolution catalyzed by activities from mammalian cells. *Cell*, 104, 259-268.
18. Wood, R. D., Mitchell, M., Sgouros, J. & Lindahl, T. (2001). Human DNA repair genes. *Science*, 291, 1284-1289.
19. Ikura, T., Ogryzko, V. V., Grigoriev, M., Groisman, R., Wang, J., Horikoshi, M. *et al.* (2000). Involvement of the TIP60 histone acetylase complex in DNA repair and apopotosis. *Cell*, 102, 463-473.
20. Shen, X., Mizuguchi, G., Hamiche, A. & Wu, C. (2000). A chromatin remodeling complex involved in transcription and DNA processing. *Nature*, 406, 541-544.
21. Tong, J. & Wetmur, J. G. (1996). Cloning, sequencing, and expression of *ruvB* and characterization of RuvB proteins from two distantly related thermophilic eubacteria. *J. Bacteriol.* 178, 2695-2700.
22. Neuwald, A. F., Aravind, L., Spouge, J. L. & Koonin, E. V. (1999). AAA+: A class of chaperone-like ATPases associated with the assembly, operation, and disassembly of protein complexes. *Genome Res.* 9, 27-43.
23. Gajiwala, K. S. & Burley, S. K. (2000). Winged helix proteins. *Curr. Opin. Struct. Biol.* 10, 110-116.
24. Iwasaki, H., Han, Y. W., Okamoto, T., Yoshikawa, M., Yamada, K., Toh, H. *et al.* (2000). Mutational

analysis of the function motifs of RuvB, an AAA+ class helicase and motor protein for Holliday junction branch migration. *Mol. Microbiol.* 36, 528-538.
25. Yamada, K., Kunishima, N., Mayanagi, K., Ohnishi, T., Nishino, T., Iwasaki, H. *et al.* (2001). Crystal structure of the Holliday junction migration motor protein RuvB from *Thermus thermophilus* HB8. *Proc. Natl Acad. Sci. USA*, 98, 1442-1447.
26. Walker, J. E., Saraste, M., Runswick, M. J. & Gay, N. J. (1982). Distantly related sequences in the α- and β-subunits of ATP synthase, myosin, kinases and other ATP-requiring enzymes and a common nucleotide binding fold. *EMBO J.* 1, 945-951.
27. Lenzen, C. U., Steinmann, D., Whitehart, S. W. & Weis, W. I. (1998). Crystal structure of the hexamerization domain of the N-ethylmaleimide-sensitive fusion protein. *Cell*, 94, 525-536.
28. Yu, R. C., Hanson, P. I., Jahn, R. & Brünger, A. T. (1998). Structure of the ATP-dependent oligomerization domain of the N-ethylmaleimide-sensitive factor complexed with ATP. *Nature Struct. Biol.* 5, 803-811.
29. George, H., Mezard, C., Stasiak, A. & West, S. C. (1999). Helicase-defective RuvB(D113E) promotes RuvAB-mediated branch migration *in vitro*. *J. Mol. Biol.* 293, 505-519.
30. Hishida, T., Iwasaki, H., Yagia, T. & Shinagawa, H. (1999). Role of Walker motif A of RuvB protein in promoting branch migration of Holliday junctions. Walker motif A mutations affect ATP binding, ATP hydrolyzing, and DNA binding activities of RuvB. *J. Biol. Chem.* 274, 25335-25342.
31. Guenther, B., Onrust, R., Sali, A., O'Donnell, M. & Kuriyan, J. (1997). Crystal structure of the δ' subunit of the clamp-loading complex of *E. coli* DNA polymerase III. *Cell*, 91, 335-345.
32. Yamada, K., Fukuoh, A., Iwasaki, H. & Shinagawa, H. (1999). Novel properties of the *Thermus thermophilus* RuvB protein, which promotes branch migration of Holliday junctions. *Mol. Gen. Genet.* 261, 1001-1011.
33. Sousa, M. C., Trame, C. B., Tsuruta, H., Wilbanks, S. M., Reddy, V. S. & McKay, D. B. (2000). Crystal and solution structures of an HslUV protease-chaperone complex. *Cell*, 103, 633-643.
34. Bochtler, M., Hartmann, C., Song, H. K., Bourenkov, G. P., Bartunik, H. D. & Huber, R. (2000). The structures of HslU and the ATP-dependent protease HslU-HslV. *Nature*, 403, 800-805.
35. Stasiak, A., Tsaneva, I. R., West, S. C., Benson, C. J., Yu, X. & Egelman, E. H. (1994). The *Escherichia coli* RuvB branch migration protein forms double hexameric rings around DNA. *Proc. Natl Acad. Sci. USA*, 91, 7618-7622.
36. Svergun, D. I., Volkov, V. V., Kozin, M. B. & Stuhrmann, H. B. (1996). New developments in direct shape determination from small angle scattering. 2. Uniqueness. *Acta Crystallog. sect. A*, 52, 419-426.
37. Mitchell, A. H. & West, S. C. (1994). Hexameric rings of *Escherichia coli* RuvB protein. Cooperative assembly, processivity and ATPase activity. *J. Mol. Biol.* 243, 208-215.
38. Marrione, P. E. & Cox, M. M. (1995). RuvB protein-mediated ATP hydrolysis: functional asymmetry in the RuvB hexamer. *Biochemistry*, 34, 9809-9818.
39. Yu, X. & Egelman, E. H. (1997). The RecA hexamer is a structural homologue of ring helicases. *Nature Struct. Biol.* 4, 101-104.
40. Singleton, M. R., Sawaya, M. R., Ellenberger, T. & Wigley, D. B. (2000). Crystal structure of T7 gene 4 ring helicase indicates a mechanism for sequential hydrolysis of nucleotides. *Cell*, 101, 589-600.
41. Karata, K., Inagawa, T., Wilkinson, A. J., Tatsuta, T. & Ogura, T. (1999). Dissecting the role of a conserved motif (the second region of homology) in the AAA family of ATPases. *J. Biol. Chem.* 274, 26225-26232.
42. Noel, J. P. (1997). Turning off the Ras switch with the flick of a finger. *Nature Struct. Biol.* 4, 677-680.
43. Zhang, B., Zhang, Y., Collins, C. C., Johnson, D. I. & Zheng, Y. (1999). A built-in arginine finger triggers the self-stimulatory GTPase-activating activity of Rho family GTPases. *J. Biol. Chem.* 274, 2609-2612.
44. Nadanaciva, S., Weber, J., Wilke-Mounts, S. & Senior, A. E. (1999). Importance of F_1-ATPase residue α-Arg-376 for catalytic transition state stabilization. *Biochemistry*, 38, 15493-15499.
45. Marrione, P. E. & Cox, M. M. (1996). Allosteric effects of RuvA protein, ATP, and DNA on RuvB protein-mediated ATP hydrolysis. *Biochemistry*, 35, 11228-11238.
46. George, H., Kuraoka, I., Nauman, D. A., Kobertz, W. R., Wood, R. D. & West, S. C. (2000). RuvAB-mediated branch migration does not involve extensive DNA opening within the RuvB hexamer. *Curr. Biol.* 10, 103-106.
47. Hiom, K. & West, S. C. (1995). Branch migration during homologous recombination: assembly of a RuvAB-Holliday junction complex *in vitro*. *Cell*, 80, 787-793.
48. Adams, D. E. & West, S. C. (1995). Unwinding of closed circular DNA by the *Escherichia coli* RuvA and RuvB recombination/repair proteins. *J. Mol. Biol.* 247, 404-417.
49. Muller, B., Tsaneva, I. R. & West, S. C. (1993b). Branch migration of Holliday junctions promoted by the *Escherichia coli* RuvA and RuvB proteins. II. interaction of RuvB with DNA. *J. Biol. Chem.* 268, 17185-17189.
50. Nishino, T., Iwasaki, H., Kataoka, M., Ariyoshi, M., Fujita, T., Shinagawa, H. & Morikawa, K. (2000). Modulation of RuvB function by the mobile domain III of the Holliday junction recognition protein RuvA. *J. Mol. Biol.* 298, 407-416.
51. Gonzalez, S. & Wetmur, J. G. (2000). Holliday junction branch migration and resolution. RuvA, RuvB, and RuvC from the hyperthermophile *Thermotoga maritima*. *Methods Mol. Biol.* 152, 107-118.
52. Gonzalez, S., Rosenfeld, A., Szeto, D. & Wetmur, J. G. (2000). The Ruv proteins of *Thermotoga maritima*: branch migration and resolution of Holliday junctions. *Biochim. Biophys. Acta*, 1494, 217-225.
53. Otwinowski, Z. (1993). Data collection and processing. In *Proceedings of the CCP4 Study Weekend* (Sawyer, L., Isaacs, N. & Bailey, S., eds), pp. 56-62. Science and Engineering Research Council, Warrington.
54. Collaborative Computational Project Number 4 (1994). The CCP4 suite: programs for protein crystallography. *Acta Crystallog. sect. D*, 50, 760-763.
55. McRee, D. E. (1999). XtalView/Xfit - a versatile program for manipulating atomic coordinates and electron density. *J. Struct. Biol.* 125, 156-165.
56. Brünger, A. T., Adams, P. D., Core, G. M., Delano, W. L., Gros, P., Grosse-Kunstleve, R. W. *et al.* (1998). Crystallography & NMR system: a new software

suite for macromolecular structure determination. *Acta Crystallog. sect. D*, 54, 905-921.
57. Brünger, A. T. (1993). Assessment of phase accuracy by cross validation: the free *R* value. Methods and applications. *Acta Crystallog. sect. D*, 49, 24-36.
58. Svergun, D. I. (1993). A direct indirect method of small-angle scattering data treatment. *J. Appl. Crystallog.* 26, 258-267.
59. Svegun, D. I. & Stuhrmann, H. B. (1991). New developments in direct shape determination from small angle scattering. 1. Theory and model calculations. *Acta Crystallog. sect. A*, 47, 736-744.
60. Svergun, D. I., Barberato, C. & Koch, M. H. J. (1995). CRYSOL - a program to evaluate X-ray solution scattering of biological macromolecules from atomic coordinates. *J. Appl. Crystallog.* 28, 768-773.
61. White, A., Ding, X., van der Spek, J. C., Murphy, J. R. & Ringe, D. (1998). Structure of the metal-ion-activated diphtheria toxin repressor/tox operator complex. *Nature*, 394, 502-506.
62. Ariyoshi, M., Vassylyev, D. G., Iwasaki, H., Nakamura, H., Shinagawa, H. & Morikawa, K. (1994). Atomic structure of the RuvC resolvase: a Holliday junction-specific endonuclease from *E. coli*. *Cell*, 78, 1063-1072.

Edited by T. Richmond

(Received 14 March 2001; received in revised form 11 June 2001; accepted 11 June 2001)